JACS
JOURNAL OF THE AMERICAN CHEMICAL SOCIETY
Article
pubs.acs.org/JACS

Gold–Gold Bonding: The Key to Stabilizing the 19-Electron Ternary Phases *Ln*AuSb (*Ln* = La–Nd and Sm)

Elizabeth M. Seibel,* Leslie M. Schoop, Weiwei Xie, Quinn D. Gibson, James B. Webb, Michael K. Fuccillo, Jason W. Krizan, and Robert J. Cava*

Department of Chemistry, Princeton University, Princeton, New Jersey 08544, United States

Supporting Information

ABSTRACT: We report a new family of ternary 111 hexagonal *Ln*AuSb (*Ln* = La–Nd, Sm) compounds that, with a 19 valence electron count, has one extra electron compared to all other known *Ln*AuZ compounds. LaAuSb, CeAuSb, PrAuSb, NdAuSb, and SmAuSb crystallize in the YPtAs-type structure, and have a doubled unit cell compared to other *Ln*AuZ phases as a result of the buckling of the Au–Sb honeycomb layers to create interlayer Au–Au dimers. The dimers accommodate the one excess electron per Au and thus these new phases can be considered $Ln_2^{3+}(Au–Au)^0Sb_2^{3-}$. Band structure, density of states, and crystal orbital calculations confirm this picture, which results in a nearly complete band gap between full and empty electronic states and stable compounds; we can thus present a structural stability phase diagram for the *Ln*AuZ (Z = Ge, As, Sn, Sb, Pb, Bi) family of phases. Those calculations also show that LaAuSb has a bulk Dirac cone below the Fermi level. The YPtAs-type *Ln*AuSb family reported here is an example of the uniqueness of gold chemistry applied to a rigidly closed shell system in an unconventional way.

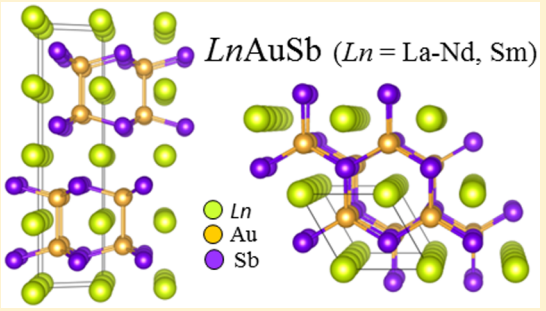

INTRODUCTION

Significant structural variety exists among gold-based ternary intermetallic compounds of the 1:1:1 *Ln*AuZ type, where *Ln* = a lanthanide and Z = a heavy main group element (Ge, As, Sn, Sb, Pb, Bi). The compounds typically crystallize in two distinct, but related structures: the cubic half-Heusler structure and the hexagonal LiGaGe structure.[1,2] More complex variants among the hexagonal phases are also known.[2−4] Both the Half-Heusler and hexagonal compounds of the form *AYZ* can be thought of as a $(YZ)^{n-}$ lattice stuffed with A^{n+} cations. Using the electron-counting system employed by Bojin and Hoffmann,[2,3] the electropositive rare earth atoms are ionic in nature and donate their electrons to the more electronegative (*YZ*) network in a Zintl-like fashion (the *f* electrons are highly localized and do not contribute). The transition metal *Y* is counted as providing both *s* and *d* electrons, and the main group atom *Z* contributes its outer shell *s* and *p* electrons. The hexagonal structures, which are the focus of this report, are built from sheets of Y_3Z_3 hexagons in a honeycomb array. The stacking sequences and degree of *YZ* buckling lead to varying degrees of interlayer bonding, that is, through the formation of *Y*–*Z*, *Y*–*Y*, or *Z*–*Z* bonds between honeycomb layers (see Figure 1). This results in structures that range from simple 2-layer structures (i.e., CeAuGe, CeAuSn, CeAuPb, etc.)[5−7] to orthorhombically distorted, complex 10-layer structures (i.e., EuAuSn).[2] Representative hexagonal structure types in this family are shown in Figure 1. In general, ternary *LnYZ* phases are of interest because they can exhibit interesting magnetic and electronic properties from unpaired transition metal electrons and from localized, rare-earth *f* electrons.[2,3]

Despite the wide structural variety within the hexagonal compounds in this 111 *AYZ* family, the rare-earth-containing compounds are nearly always 18 valence electron systems, giving filled bonding orbitals.[1] While half-Heusler compounds with 18 electrons are typically semiconducting, hexagonal *AYZ* compounds with 18 electrons can range from semiconductors to semimetals with nearly complete band gaps between filled and occupied states, depending on the extent of the *YZ* layer buckling.[1] We present here a new hexagonal family of *Ln*AuSb (*Ln* = La–Nd, Sm) compounds that crystallizes in a 4-layer structure of the YPtAs-type.[8] These new phases have 19 valence electrons; this is highly unusual as it implies that metal antibonding orbitals would be populated in typical 111 hexagonal structures. We show, however, that the 19th electron is localized in a molecular-like, interlayer Au–Au dimer bond, resulting in a nearly complete band gap between filled bonding states and empty antibonding states, and thus chemical stability. The compounds should therefore be considered as $Ln_2^{3+}(Au–Au)^0Sb_2^{3-}$ phases. Their electronic relationship to other *Ln*AuZ phases is described.

EXPERIMENTAL SECTION

Syntheses. As starting materials, 99.9% purity rare earth and >99.99% purity other metals were used. The rare earth elements were

Received: November 5, 2014
Published: December 26, 2014

DOI: 10.1021/ja511394q
J. Am. Chem. Soc. 2015, 137, 1282–1289

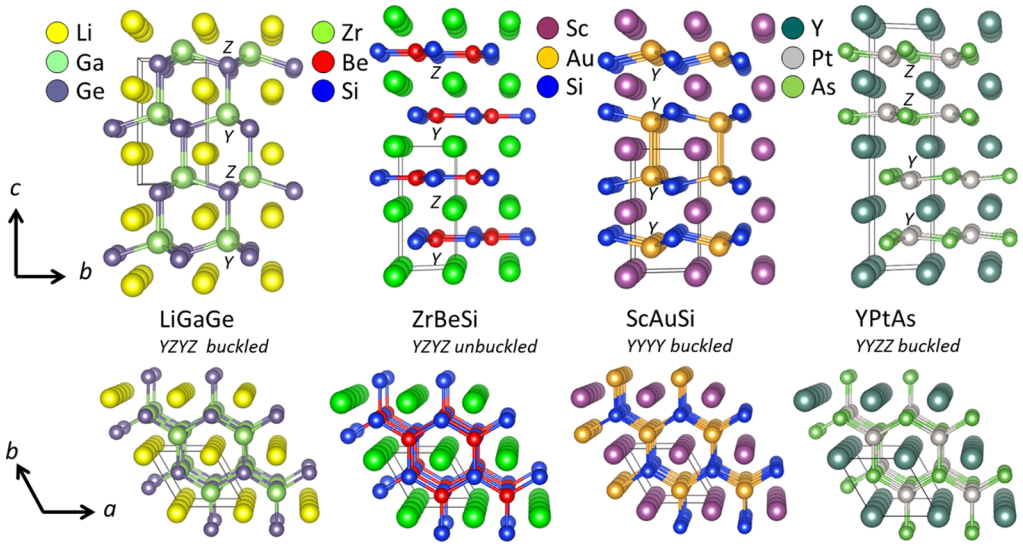

Figure 1. Crystal structures of the archetype hexagonal 111 compounds LiGaGe, ZrBeSi, ScAuSi, and YPtAs. The top panel illustrates the stacking along *c*; the bottom panel demonstrates the honeycomb Y_3Z_3 nets in the *a*−*b* plane. LiGaGe and ZrBeSi are 2-layer honeycomb structures that stack with alternating *YZYZ* atoms along *c*, but LiGaGe has buckled Y_3Z_3 honeycomb layers whereas ZrBeSi is flat. ScAuSi is also a buckled, 2-layer structure, but with *YYYY* stacking to allow for interlayer *Y*−*Y* contacts. YPtAs is a slightly buckled 4-layer structure with *YYZZ*-type stacking along *c*, such that extensive buckling of the Y_3Z_3 layers could allow for *Y*−*Y* interlayer bonds.

arc melted before use and stored in an inert atmosphere. For *Ln*AuSb compounds, the rare earth, $AuSb_2$ (made by melting at 850 °C), and Au were used as starting materials to minimize Sb vaporization on arc melting. These starting materials were arc melted in argon in a 1:1:1 Ln:Au:Sb stoichiometry. Samples were then annealed in evacuated silica tubes for 48 h at 850 °C. Longer annealing times or hotter annealing temperatures caused decomposition into $Ln_3Au_3Sb_4$, and the use of excess Sb during arc melting led to the formation of impurity phases. We also synthesized LaAuSn for comparison purposes (as described below) by arc melting the elements in an argon atmosphere in a 1:1:1 ratio and then annealing at 850 °C for 1 week. The arc melted buttons were stable in air for days, but sample grinding was carried out in an inert atmosphere to prevent rapid oxidation.

X-ray Powder Diffraction. Samples were initially checked for phase purity by powder X-ray diffraction (pXRD) using a Rigaku MiniFlex II instrument with Cu Kα radiation and a diffracted beam monochromator. Synchrotron powder X-ray diffraction data for structure refinement was collected at beamline 11-BM at the Advanced Photon source at Argonne National Laboratory for LaAuSb, CeAuSb, and NdAuSb at 298 K. The resulting powder diffraction patterns were refined using the FullProf suite. Small single crystals of LaAuSb and LaAuSn were selected from the arc melted buttons for single crystal study. Single crystals were mounted on the tips of glass fibers, and room temperature intensity data were collected on a Bruker Apex II diffractometer with Mo radiation Kα_1 (λ = 0.71073 Å). Data were collected over a full sphere of reciprocal space with 0.5° scans in ω with an exposure time of 20s per frame. The 2θ range extended from 4° to 60°. The SMART software was used for data acquisition. Intensities were extracted and corrected for Lorentz and polarization effects with the SAINT program. Empirical absorption corrections were accomplished with SADABS which is based on modeling a transmission surface by spherical harmonics employing equivalent reflections with $I > 2\sigma(I)$.[9,10] The crystal structure of LaAuSn was solved using direct methods and refined by full-matrix least-squares on F^2 using the SHELX package.[11] All crystal structure drawings were produced using the program VESTA.[12]

Structure Determinations. Rietveld refinements of synchrotron X-ray powder diffraction data were carried out for LaAuSb, CeAuSb, and NdAuSb. $Ln_3Au_2Sb_3$, $Ln_{14}Au_{51}$, and $Ln_3Au_3Sb_4$ impurity phases were observed. To the best of our knowledge, of the $Ln_3Au_2Sb_3$ phases only $Ce_3Au_2Sb_3$ has been reported.[13] Because all samples contained at least one impurity phase, the composition of the *Ln*AuSb phases was fixed in the 1:1:1 stoichiometry in the refinements. The atomic positions for YPtAs were used as starting points for the powder refinements; different models were tested with variations of the Au and Sb positions and extent of honeycomb buckling; all refinements quickly converged. Full structure solutions for PrAuSb and SmAuSb were not attempted due to the presence of significant amounts of the $Ln_3Au_3Sb_4$ impurity phase, but their unit cell parameters were easily determined.

The structure of LaAuSn was previously reported as a disordered version of the LiGaGe type with Au/Sn mixing (the $CaIn_2$-type);[14] however, we find that the compound crystallizes in the ordered, 2-layer LiGaGe-type, in agreement with other *Ln*AuSn phases.[15] Relevant structure parameters refined from single crystal data for LaAuSn are given in Tables S1 and S2, Supporting Information.

Electronic Calculations. The electronic structure of LaAuSb was calculated with the aid of CAESAR,[16] according to semiempirical extended-Hückel-tight-binding (EHTB) methods. The parameters for Au are 6*s*: ζ = 1.890, H_{ii} = −8.23 eV; 6*p*: ζ = 1.835, H_{ii} = −4.89 eV, and 5*d*: ζ = 3.560, H_{ii} = −12.200 eV. The Au parameters were modified to provide the best fit to the results of first-principles calculations with relativistic effects.[17,18] Partial density of states (DOS) and crystal orbital Hamilton population (COHP) calculations[19] were performed by the self-consistent, tight-binding, linear-muffin-tin-orbital (LMTO) method in the local density (LDA) and atomic sphere (ASA) approximations, within the framework of the DFT method.[20−22] Interstitial spheres were introduced in order to achieve space filling. The ASA radii as well as the positions and radii of these empty spheres were calculated automatically, and the values so obtained were all reasonable. Reciprocal space integrations were carried out using the tetrahedron method. Down-folding techniques were automatically applied to the LMTOs, and scalar relativistic effects were included in the calculations.

Further, ab initio electronic band structure calculations were performed in the framework of density functional theory (DFT) using the WIEN2k[23] code with a full-potential linearized augmented plane-wave and local orbitals [FP-LAPW + lo] basis[24−26] together with the Perdew−Becke−Ernzerhof (PBE) parametrization[27] of the generalized gradient approximation (GGA) as the exchange-correlation functional. The plane wave cutoff parameter $R_{MT}K_{MAX}$ was set to 8, and the Brillouin zone was sampled by 2000 k-points. Experimental lattice parameters from the Rietveld refinements (for LaAuSb and LaAuSn) and from published data (LaAuPb)[28] were used

DOI: 10.1021/ja511394q
J. Am. Chem. Soc. 2015, 137, 1282−1289

in the calculations. Spin orbit coupling (SOC) and relativistic effects were included.

RESULTS AND DISCUSSION

Structural Description. Among the *Ln*AuSb (*Ln* = La−Nd, Sm) phases, CeAuSb was previously known to exist but its structure was undetermined. The powder X-ray diffraction data was interpreted as indicating a 2-layer, disordered LiGaGe-type structure (Figure 1), but with impurity phases present.[29] In a more recent study of the Ce−Au−Sb phase diagram, the existence of CeAuSb was confirmed by SEM-EDS, but the observed powder diffraction pattern was found to be inconsistent with the previously reported structure.[13] In our investigation of *Ln*AuSb (*Ln* = La−Nd, Sm) phases, we found that a small single crystal selected from an arc melted button of LaAuSb rather had twice the *c*-axis previously reported for CeAuSb, as expected for the 4-layer YPtAs structure type (Figure 1). Inspection of the CeAuSb powder diffraction pattern then subsequently showed that peaks previously associated with impurity phases, present in all the *Ln*-phases reported here, are in fact captured by a doubling of the *c*-axis, that is, by a 4-layer rather than a 2-layer structure. Thus, we determined that a four layer structural pattern, rather than a two-layer pattern, describes the crystal structures of the light rare earth compounds in the *Ln*AuSb family. The single crystal data was not of sufficient quality to perform a full structural study, and therefore the structures were determined quantitatively from the synchrotron powder X-ray diffraction data. The powder pattern and fit to the data for LaAuSb is shown in Figure 2 as an example (see Supporting Information Figures S1 and S2 for CeAuSb and NdAuSb). Table 1 gives the lattice parameters for all the *Ln*AuSb (*Ln* = La−Nd, Sm) phases observed in this study, and Table 2 gives the refined structural parameters for LaAuSb, CeAuSb, and NdAuSb.

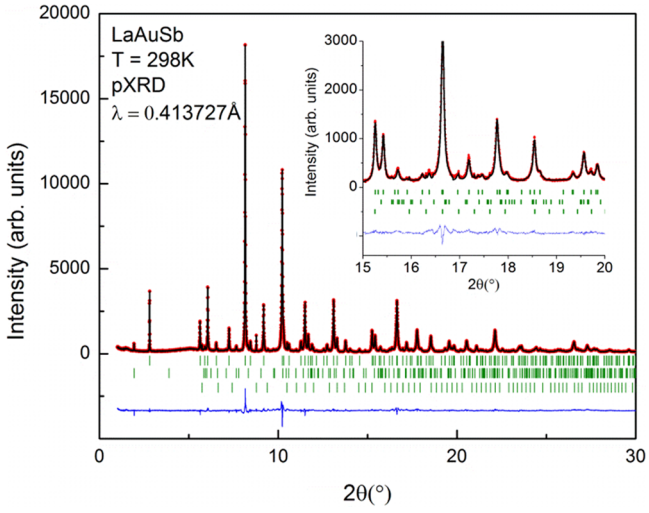

Figure 2. Rietveld refinement of LaAuSb. Observed synchrotron powder X-ray diffraction data is shown in red, calculated in black, and the difference ($Y_{obs} - Y_{calc}$) in blue. The insets show the peak shapes and fit to the data from 15 to 20° 2θ. Green tick marks are Bragg reflections for LaAuSb (top), $La_3Au_2Sb_3$ (middle), and $La_3Au_3Sb_4$ (bottom).

Figure 3 shows the refined structure of LaAuSb, and Figure 4 compares this to the archetype YPtAs. In the YPtAs structure type, the only variable positional coordinates are the *z*-axis parameters of the Pt and As sites that form the Y_3Z_3 honeycomb layers. These parameters reflect the degree of layer buckling and thus the degree of *Y*−*Y* interlayer bonding; for the current materials, this is a Au−Au bond. As can be seen in the figure, the *Ln*AuSb phases are more buckled than the YPtAs prototype, and in that respect are similar to LiGaGe. However, in the LiGaGe structure type, the honeycomb layers are arranged so that the *Y* and *Z* atoms are above each other resulting in *Y*−*Z* interlayer bonding and *Y*−*Y* interlayer bonding is not possible. However, in the YPtAs structure type observed for our *Ln*AuSb phases, the neighboring honeycomb layers alternate their stacking in a ...*YYZZYYZZ*... arrangement and buckle (Figure 1), which we attribute to the Au−Au bond formation. The resulting coordination polyhedra and selected bond lengths for LaAuSb are shown in Figure 3, and Table S3 summarizes the interatomic bond lengths for LaAuSb, CeAuSb, and NdAuSb. In all compounds, the rare earth atoms adopt 12-fold coordination, whereas the Sb atoms form a trigonal prism with *Ln*. Three bent Au−Sb bonds cut through this prism. If the Au−Au dimer is treated as one unit, it adopts 9-fold coordination made of a Sb trigonal prism with planar trigonal *Ln* bonds. The near neighbor coordination polyhedra are generally the same in shape in LiGaGe structure type compounds, but the atoms found at the vertices are different.

Though the cutoff for bonding is somewhat arbitrary, here we consider interactions less than 3.15 Å to be a covalent bond for Au−Au contacts.[2] In *Ln*AuSb (*Ln* = La−Nd, Sm), the honeycomb layer buckling allows the gold atoms in neighboring planes to approach each other at a distances of 2.98, 3.05, and 3.12 Å for Nd, Ce, and La, respectively (see Table S3 for selected bond distances). In contrast, the intralayer Au−Sb bond length is nearly constant at 2.77−2.78 Å. Thus, the primary influence of the size of the rare earth ion is to modulate the spacing between the honeycomb layers. The Au−Au interlayer bonds of ∼3−3.1 Å are longer than the bonding in metallic gold (2.88 Å), but they are squarely within the range of "aurophilic interactions" (2.8−3.5 Å).[30]

The term "aurophilic interaction" is most strictly used to describe the affinity between two closed-shell gold centers (Au^{1+}, $5d^{10}$) driven by relativistic effects and the high electronegativity of gold.[30] In molecular systems, these aurophilic interactions can often be significant enough to drive dimerization (e.g., for $[(Me_2PCH_2PMe_2)_3Au_2]^+$) and crystallization (e.g., for 1,1′-di(isocyano)ferrocene).[30] The term is also often applied to mixed-valence interactions (between $Au^{1-}[6s^25d^{10}]$, $Au^0[6s^15d^{10}]$, and/or Au^{1+} $[5d^{10}]$) in molecules, but for these types of open-shell interactions (like Au^0−Au^{1+}) the aurophilicity may have a smaller impact on cluster formation and a description in terms of metal−metal bonding may be more appropriate.[30] The tendency for gold to form auride anions in the solid state due to its high electronegativity has also previously discussed from a Zintl perspective for compounds like CsAu and Cs_3AuO.[31] Weak gold−gold interactions have been observed in other hexagonal 111 phases such as UAuGe (Au−Au = 3.27 Å), which crystallizes in the YPtAs structure, and in ScAuSi (Au−Au = 2.94 Å) which has its own hexagonal structure type with Au−Au bonds (see Figure 1).[32,33] Additionally, the Au−Au contacts in EuAuGe (Au−Au = 3.16 Å) are suggested to arise from realtivistic interactions.[34] Weak, secondary Au−Au and Sn−Sn interactions are also important driving factors for the formation of a KHg_2-type superstructure for YbAuSn (Au−Au = 3.32 Å).[35] Because the

DOI: 10.1021/ja511394q
J. Am. Chem. Soc. 2015, 137, 1282−1289

Table 1. Crystal Data and Structure Refinements for LnAuSb (Ln = La−Nd, Sm)

formula	LaAuSb[a]	CeAuSb[a]	PrAuSb[b]	NdAuSb[a]	SmAuSb[b]
formula weight (g/mol)	457.63	458.84	459.63	462.97	469.09
space group	$P6_3/mmc$	$P6_3/mmc$	$P6_3/mmc$	$P6_3/mmc$	$P6_3/mmc$
Z	2	2	2	2	2
unit cell (Å)					
a	4.63838(6)	4.6140(1)	4.593(2)	4.5800(1)	4.551(2)
c	16.8315(4)	16.6348(6)	16.532(1)	16.4775(5)	16.398(1)
volume	313.60(1)	306.66(1)	302.13(3)	299.34(1)	294.21(3)
χ^2	3.00	4.91	3.05	3.92	2.67
R_{wp}	14.4	13.5	28.2	13.8	26.4
R_p	13.9	12.4	26.6	12.7	23.5
impurity phases	$La_3Au_2Sb_3$	$Ce_3Au_2Sb_3$	$Pr_3Au_2Sb_3$	$Nd_3Au_2Sb_3$	$Sm_3Au_3Sb_4$
	$La_3Au_3Sb_4$	$Ce_{14}Au_{51}$	$Pr_{14}Au_{51}$	$Nd_{14}Au_{51}$	$Sm_{14}Au_{51}$

[a]Rietveld refinement from synchrotron data. [b]Profile fit from lab PXRD.

Table 2. Atomic Coordinates and Thermal Parameters for LnAuSb (Ln = La, Ce, Nd) Phases

phase	atom	Wyckoff	x	y	z	B_{iso}	occ.
LaAuSb	La1	2*a*	0	0	0	0.86(6)	1
	La2	2*b*	0	0	1/4	0.86(6)	1
	Au1	4*f*	2/3	1/3	0.1572(1)	1.34(4)	1
	Sb1	4*f*	1/3	2/3	0.1127(2)	0.78(7)	1
CeAuSb	Ce1	2*a*	0	0	0	0.9(1)	1
	Ce2	2*b*	0	0	1/4	0.9(1)	1
	Au1	4*f*	2/3	1/3	0.1583(2)	1.24(7)	1
	Sb1	4*f*	1/3	2/3	0.1122(4)	0.8(1)	1
NdAuSb	Nd1	2*a*	0	0	0	0.8(1)	1
	Nd2	2*b*	0	0	1/4	0.8(1)	1
	Au1	4*f*	2/3	1/3	0.1596(2)	1.09(7)	1
	Sb1	4*f*	1	1/3	2/3	0.8(1)	1

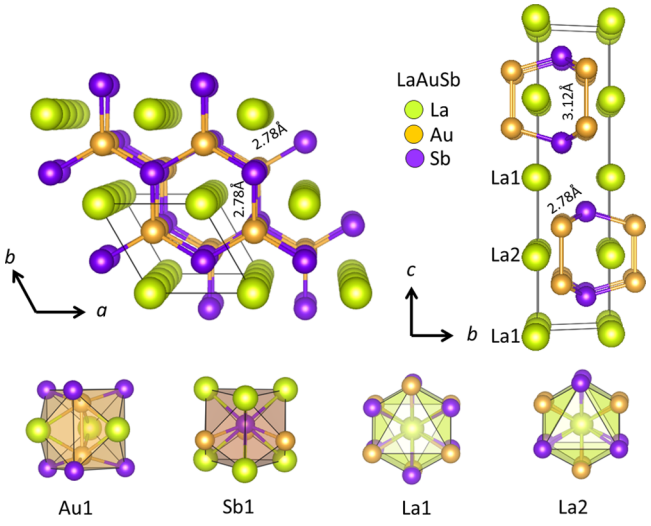

Figure 3. Structure of LaAuSb. CeAuSb and NdAuSb are isostructural; we assume the same for PrAuSb and SmAuSb based on their crystallographic cell parameters. The Au_3Sb_3 hexagonal layers are easily visible in a−b projection, shown in the top left. The top right shows the projection of the b−c plane. Au−Sb and Au−Au bond lengths are indicated on the figure. The bottom portion shows the coordination polyhedra for Au, Sb, and the two La sites. If the Au−Au dimer is treated as a unit, the dimer adopts 9-fold coordination formed by a Sb trigonal prism and trigonal planar La bonds. Sb has trigonal prismatic coordination with La through which there are three bent Au bonds. Both La display dodecahedral coordination, though with different Au and Sb at the vertices.

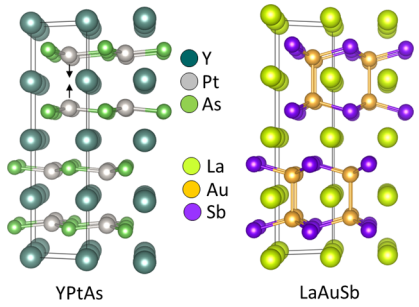

Figure 4. Structure comparisons of YPtAs (left) and LaAuSb (right). Although LaAuSb adopts the YPtAs structure type, the Au and Sb atoms are significantly more buckled than the Pt and As atoms in the archetypical structure, which is a signature of the Au−Au interlayer bonding. The black arrows in the figure are meant to indicate the direction of motion of the As site to allow for interlayer Au−Au bond formation.

Au−Au interlayer contacts in *Ln*AuSb are even shorter than these (Au−Au = 2.98−3.12 Å), it is likely that the structure of the *Ln*AuSb compounds described here is driven by these gold−gold interactions.

Electronic Structure Calculations. To gain further insight into the bonding interactions in LaAuSb, we performed several types of electronic structure calculations. Figure 5 shows the density-of-states (DOS) curves with Au 6*s*, 5*d*, and 6*p* states highlighted, as well as the crystal orbital Hamilton population (COHP) data calculated (LMTO) for LaAuSb (see Table S4 for −ICOHP parameters). A prominent feature in the DOS is the strong suppression of states (pseudogap) at the Fermi level

DOI: 10.1021/ja511394q
J. Am. Chem. Soc. 2015, 137, 1282−1289

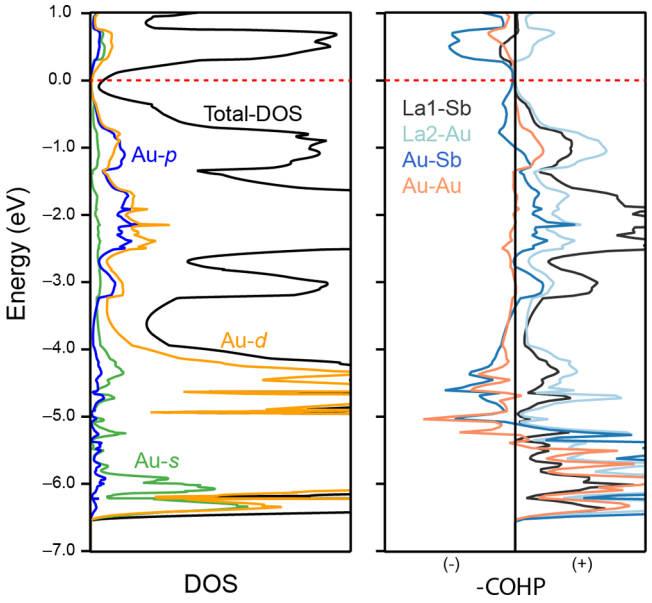

Figure 5. DOS and COHP for LaAuSb calculated using LMTO. The gold 6*s*, 5*d*, and 6*p* states that contribute to the total DOS are highlighted on the left. La1−Sb, La2−Au, Au−Sb, and Au−Au interactions are highlighted in the COHP, shown on right. The gold 6*s* and 5*d* states are highly localized between −4 and −6.5 eV in the DOS plot, which creates bonding interactions (−6.5 to −5 eV) and antibonding interactions (−5 to −3 eV) seen in the COHP. The overall bonding interactions from approximately −4 to −1.5 eV are made of hybridized Au, Sb, and La states. The compound is nonbonding in the COHP from ±1 eV around the indicated Fermi level, which sits in a deep depression of the density of states, a "pseudogap".

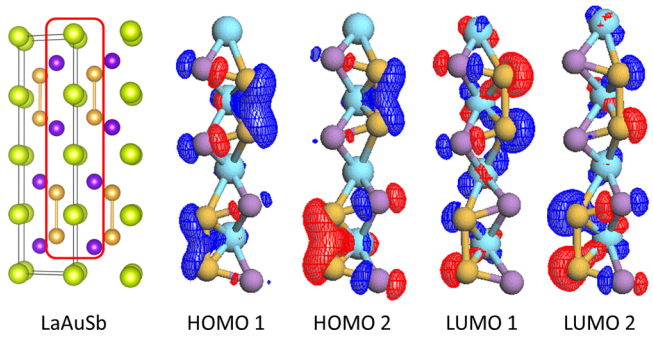

Figure 6. HOMOs and LUMOs of LaAuSb calculated using extended Hückel theory with relativistic effects included. The unit cell of LaAuSb is shown for comparison with Au−Au bonds; the red outline indicates the part of the crystal structure shown in the MO calculations. The sign of the wave function is indicated by red and blue color. The strong orbital overlap between interlayer Au atoms creates a bond in which two electrons (one from each Au) are localized.

together with empty La−Au, La−Sb, and Au−Au bonding states, while Au−Sb states are antibonding just below E_F. Within ±1 eV of the indicated E_F, the overall COHP is nonbonding; the location of the E_F is favored by the low DOS. This indicates that 19 valence electrons optimize the bonding of the whole compound. Most of the DOS curve between −7 to −4 eV below the Fermi level belongs to the Au-5*d* and Au-6*s* electrons. The Au states (*s*, *p*, and *d*) from −3.5 to 0 eV integrate to ∼0.95 electrons per gold; this corresponds to the gold−gold interlayer bond. Above −3 eV, most contribution to the DOS comes from Sb 5*p* electrons and La 6*s* and 5*d* electrons (the *f* states are treated as highly localized). This part of the DOS contains hybridized Au−Sb and La−Sb interactions according to the corresponding COHP curves, as one would expect for the covalently bonded, hexagonal Au−Sb net.

Extended Hückel theory was then applied using Slater-type zeta functions. Figure 6 illustrates the highest occupied molecular orbitals (HOMOs) and lowest unoccupied molecular orbitals (LUMOs) for LaAuSb, which provide an interpretation for how the Au−Au dimers bond in LaAuSb. Those orbitals have contributions from Au 6*s*, 5*d*, and 6*p* orbitals, consistent with the DOS and COHP calculations discussed above. The electrons in the Au bond are more "molecular" than bandlike in nature, in the sense that they reside primarily between the Au atoms. This dimerization provides electronic stability to LaAuSb through its facilitation of a nearly complete electronic band gap between filled and empty states. The valence electrons of LaAuSb are counted as 3 (La^{3+}) + 11 (Au^0) + 5 (Sb^{3-}) = 19 electrons, which would be unstable in a LiGaGe-type compound as antibonding states would be populated. However, that is not the case in the current structure type since one extra electron per Au is in the localized Au−Au dimers according to the integrated DOS; the remaining 18 electrons yield a nearly fully gapped band structure similar to that seen in other 111 hexagonal phases. This family can therefore be viewed as $Ln_2^{3+}(Au{-}Au)^0Sb_2^{3-}$. Within the same (YPtAs) structure type, several nongold containing 19-electron systems are known to exist. These include Ln^{3+}ZnSn,[36] Ln^{3+}ZnGe,[37] and Ln^{3+}ZnPb.[38] The 19-electron germanide series shows no interlayer bonding interaction, and the stannides show weak Zn−Zn bonding.[37] Our calculations illustrate that the electronic structures of YPtAs-type phases can best be interpreted using a combination of "molecular orbital" and band electron perspectives, and not just via the nearly free electron band model.

We now compare the ab initio electronic band structure calculations for LaAuSn and LaAuSb generated using WIEN2k. Figure 7 shows both the band structures and the density of states (DOS) for LaAuSn and LaAuSb (see Supporting Information Figure S3 for similar calculations on LaAuPb). LaAuSn is a semimetal with a very strong suppression in the electronic density of states at the Fermi level (a "psdudo-gap"), straightforwardly consistent with its 18 valence electron count. This character can be simply understood by the fact that it is a charge-balanced compound; we therefore expect semiconducting or semimetallic (when the degree of covalency in the bonding is high and there is a nearly complete but not quite complete energy gap between the valence band and conduction band) behavior. If the Au atoms in *Ln*AuSb (*Ln* = La−Nd, Sm) form dimers as described here, with the one extra electron accommodated in a localized Au-dimer orbital, then we expect a strong suppression of the density of states and a pseudogap at the Fermi level since they will also be charge-balanced. From the calculations, we indeed find this to be the case, in agreement with the DOS calculations derived from the LMTO calculation. The appearance of the nearly fully gapped electronic structure of LaAuSb, where there is only one place in the Brillouin zone that is not gapped out, is therefore yet another indication for the presence of a true Au−Au bond between the layers. We note that there is bulk Dirac cone approximately 0.1 eV below the Fermi level in the Γ−A direction. This cone, along with the band crossing that creates a small DOS at E_F, is protected by the C_3 and C_6 symmetries

DOI: 10.1021/ja511394q
J. Am. Chem. Soc. 2015, 137, 1282−1289

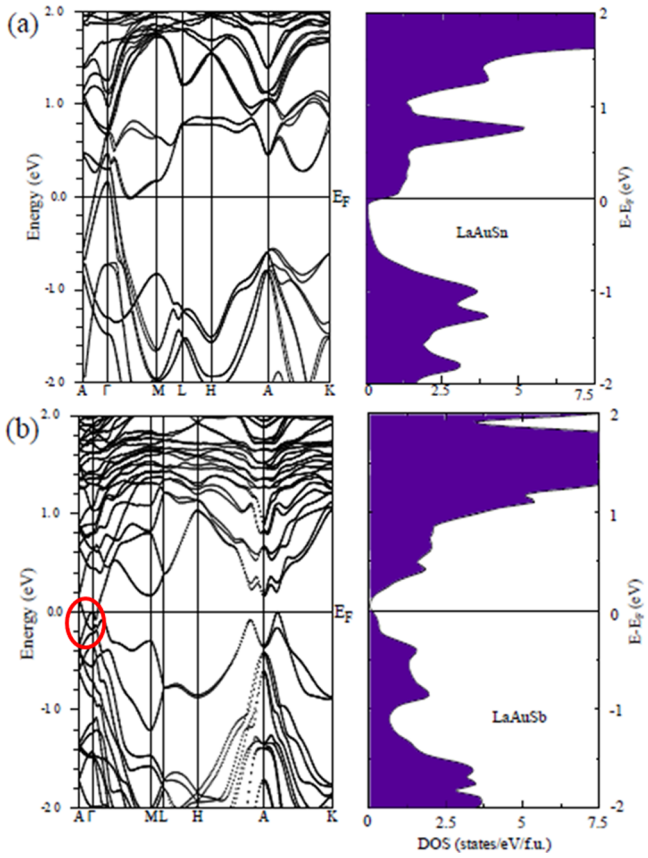

Figure 7. Ab initio electronic band structures (spin orbit coupling included) and DOS of LaAuSn (a) and LaAuSb (b). The compounds have semimetallic electronic structures, with nearly a full band gap between occupied and empty states. LaAuSb (b) has a bulk Dirac cone approximately 0.1 eV below the Fermi level in the Γ−A direction that is symmetry-protected (circled in red); this protection gives rise to the small valence band-conduction band overlap near the gamma point in the Brillouin zone.

along this line and cannot be gapped without a structural distortion to lower crystal symmetry or change in band overlap due to a significant change in lattice size.[39] Materials with bulk Dirac cones, or "Dirac semimetals", have been of recent interest due to their exotic physical properties such as extremely high carrier mobility.[40]

***Ln*AuZ Phase Comparisons.** To help place the *Ln*AuSb phases reported here in context with all other *Ln*AuZ phases, we compiled the *Ln*AuX compounds known to exist as of the time of this publication. The results are summarized in Figure 8,[5−7,15,28,41−49] where the *Y*-axis is the Ln^{3+} ionic radius and the *X*-axis is the sum of the Au*Z* metallic radii, as has been done for other 111 compounds.[50] To remind the reader, LiGaGe and YPtAs are both buckled hexagonal structures, ZrBeSi is a 2-layer unbuckled hexagonal structure, MgAgAs is the prototypical cubic half-Heusler structure, and the KHg_2-type compounds are orthorhombically distorted superstructures of stacked honeycombs.[34,35,51]

Several observations can be made. First, the Ln^{3+}AuSb systems are the only *Ln*AuZ phases known to crystallize in the YPtAs structure type, and there appear to be no other 19-electron *Ln*AuZ systems. The *Ln*AuGe, *Ln*AuSn, and *Ln*AuPb compounds, of which there are many, are all 18-electron systems for Ln^{3+}. Of the remaining *Ln*AuAs, *Ln*AuSb, and *Ln*AuBi phases the only phases known to exist besides the

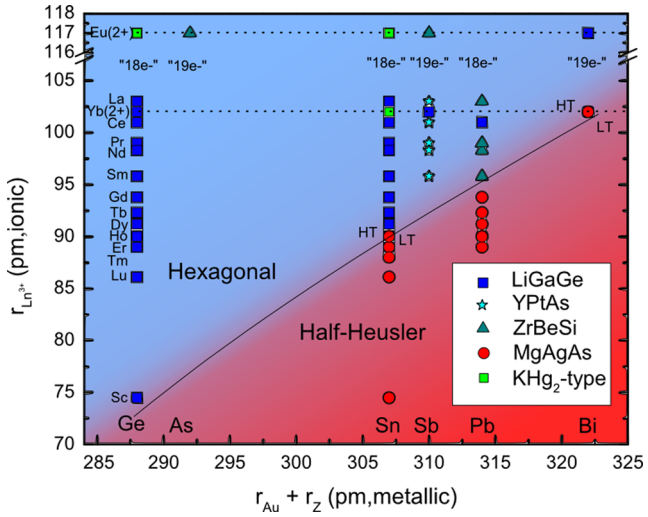

Figure 8. Structural stability phase diagram of *Ln*AuZ phases (*Z* = Ge, As, Sn, Sb, Pb, Bi). The plot is an analogy to ref 50. The LiGaGe structure type is marked with blue squares, the YPtAs type with light blue stars, ZrBeSi type with teal triangles, MgAgAs (half-Heusler) with red circles, and KHg_2-type with green squares. Red shading indicates a region of cubic symmetry (i.e., half-Heusler), whereas blue shading indicates a region of hexagonal symmetry. There are several polymorphic phases that fall within a purple region. The dashed line serves as a guide to the eye for Yb^{2+} and Eu^{2+} phases, which often crystallize in a structure type that differs from the rest of the Ln^{3+}AuZ family. Each *Ln*AuZ column is indicated as "18e-" or "19e-" based on the counting scheme adopted in the text for Ln^{3+}. "HT" and "LT" stand for high-temperature and low-temperature phases, respectively. There is a clear boundary between the hexagonal and cubic 111 phases, as well as an absence of *Ln*AuAs phases.

Ln^{3+}AuSb compounds reported here are those based on the divalent rare earths (Yb and Eu), which have an 18-electron count (dashed line in Figure 8). These 18-electron phases crystallize in the LiGaGe type rather than the YPtAs type, as would be expected, since no interlayer dimer is required to hold an extra electron. Therefore, to the best of our knowledge, the YPtAs-type *Ln*AuSb reported here are a unique, 19-electron group of *Ln*AuZ phases.

Second, we observe that there is a nearly linear phase boundary between the hexagonal phases (YPtAs, LiGaGe, ZrBeSi) and the cubic half-Heusler phase. This phase boundary is consistent with that observed by Xie et al;[50] the current *Ln*AuSb system develops further the 111 structural stability diagram specific to the rare earth cation radii. To clarify the phase boundary in greater detail, we attempted to synthesize several other 111 phases, including *Ln*AuSb (*Ln* = Gd, Tb, Dy, Tm, Sc, and Y) and *Ln*AuBi (*Ln* = La, Tm), but none were found to exist within our reaction conditions. Thus, the boundary between the hexagonal and half-Heusler structure is just below Tb^{3+} for *Ln*AuSb; while this does not explain why we could not successfully synthesize "GdAuSb", it does explain why smaller-sized rare earth variants were not found to exist in a hexagonal structure phase. There appears no straightforward way to incorporate Au dimers into a variant of the half-Heusler structure to obtain a 19-electron system, explaining why Ln^{3+}AuSb and Ln^{3+}AuBi phases are not found in the half-Heusler structure type. The phase boundary in the figure suggests that hexagonal Ln^{3+}AuBi compounds may not exist, but that it may be possible to synthesize hexagonal Ln^{3+}AuAs phases. Hypothetical Ln^{3+}AuAs compounds would have 19

DOI: 10.1021/ja511394q
J. Am. Chem. Soc. 2015, 137, 1282−1289

valence electrons and therefore should have the YPtAs-type structure.

Finally, we observe the general trend that for compounds that exist as both the hexagonal and cubic variants (for example HoAuSn[42] and YbAuBi[45]), the hexagonal phase is the high-temperature phase and the cubic phase is the low-temperature phase. Though the *Ln*AuSb compounds reported here were not found to be polymorphic, this observation supports the notion that these are high-temperature phases that require rapid quenching and may have competing polymorphs at low temperatures. It also suggests that if Ln^{3+}AuAs were to be made they may be high-temperature phases.

CONCLUSIONS

We find that the new *Ln*AuSb (*Ln* = La, Ce, Nd) compounds crystallize in the YPtAs structure type via single crystal diffraction and high-resolution powder diffraction data. We also find evidence for PrAuSb and SmAuSb crystallizing in the same structure type, and report preliminary lattice parameters for those compounds. The structure of LaAuSn was reinvestigated and found to be the ordered LiGaGe-type. The *Ln*AuSb (*Ln* = La−Nd, Sm) phases are a more buckled version of the archetypical YPtAs structure, allowing for the formation of interlayer Au−Au dimers. Molecular orbital analysis for LaAuSb shows the Au−Au dimer interaction to be that of a true bond. These dimers localize the "19th" electron and are important in maintaining a stable, charge-balanced, Zintl-like phase where the bonding states are filled and the antibonding states are empty. Ab initio band structure calculations further support the Au−Au bonding interaction and indicate that these materials are semimetals with an electronic band gap over nearly the full Brillouin zone, with a bulk Dirac cone along Γ−A. We propose that these materials may therefore be of interest for further study, and predict the stability of currently unobserved Ln^{3+}AuAs phases based on our *Ln*Au*Z* structural stability diagram. The application of localized Au chemistry to other charge-balanced systems where dimerization is possible may open the door to yet-undiscovered phases, as well as the general application of the Zintl concept to the late 5*d* transition metals in the solid state.

ASSOCIATED CONTENT

Supporting Information

Powder diffraction refinements for CeAuSb and NdAuSb (Figures S1 and S2) and selected bond lengths for LaAuSb, CeAuSb, and NdAuSb (Table S3); single crystal refinement parameters for LaAuSn (Table S1) and atomic coordinates (Table S2); band structure and DOS of LaAuPb (Figure S3); ICOHP parameters for LaAuSb (Table S4); cif outputs. This material is available free of charge via the Internet at http://pubs.acs.org.

AUTHOR INFORMATION

Corresponding Authors

eseibel@princeton.edu
rcava@princeton.edu

Notes

The authors declare no competing financial interest.

ACKNOWLEDGMENTS

This research was supported by the Air Force MURI on thermoelectric materials, Grant No. FA9550-10-1-0553, and by SPAWAR Grant NN66001-11-1-4110. The authors would like to thank Dr. Jing Gu for helpful contributions.

REFERENCES

(1) Casper, F.; Seshadri, R.; Felser, C. *Phys. Status Solidi A* **2009**, *206*, 1090−1095.
(2) Bojin, M. D.; Hoffmann, R. *Helv. Chim. Acta* **2003**, *86*, 1653−1682.
(3) Bojin, M. D.; Hoffmann, R. *Helv. Chim. Acta* **2003**, *86*, 1683−1708.
(4) Hoffmann, R. D.; Pöttgen, R. *Z. Kristallogr.* **2001**, *216*, 127−145.
(5) Pöttgen, R.; Borrmann, H.; Felser, C.; Jepsen, O.; Henn, R.; Kremer, R. K.; Simon, A. *J. Alloys Compd.* **1996**, *235*, 170−175.
(6) Niepmann, D.; Pottgen, R.; Poduska, K. M.; DiSalvo, F. J.; Trill, H.; Mosel, B. D. *Z. Naturforsch., B: J. Chem. Sci.* **2001**, *56*, 1−8.
(7) Hermes, W.; Rayaprol, S.; Pöttgen, R. *Z. Naturforsch., B: J. Chem. Sci.* **2007**, *62*, 901−906.
(8) Wenski, G.; Mewis, A. *Z. Kristallogr.* **1986**, *176*, 125−134.
(9) Sheldrick, G. M. *SADABS*; University of Gottingen: Gottingen, Germany, 2001.
(10) Sheldrick, G. M. *Acta Crystallogr. A* **2008**, *64*, 112−122.
(11) *SHELXTL*; Bruker AXS Inc.: Madison, WI, 2013.
(12) Momma, K.; Izumi, F. *J. Appl. Crystallogr.* **2011**, *44*, 1272−1276.
(13) Salamakha, L. P.; Bauer, E.; Mudryi, S. I.; Goncalves, A. P.; Almeida, M.; Noel, H. *J. Alloys Compd.* **2009**, *479*, 184−188.
(14) Latka, K.; Chajec, W.; Kmiec, K.; Pacyna, A. W. J. *J. Magn. Magn. Mater.* **2001**, *224*, 241−248.
(15) Baran, S.; Hofmann, M.; Leciejewicz, J.; Slaski, M.; Szytula, A.; Zygmunt, A. *J. Phys.: Condens. Matter* **1997**, *9*, 9053−9063.
(16) Ren, J.; Liang, W.; Whangbo, M. H. *CAESAR for Windows*; Prime-Color Software, Inc.: Raleigh, NC, 1998.
(17) Komiya, S.; Albright, T. A.; Hoffmann, R.; Kochi, J. K. *J. Am. Chem. Soc.* **1977**, *99*, 8440−8447.
(18) Xie, W. W.; Miller, G. J. *Chem. Mater.* **2014**, *26*, 2624−2634.
(19) Dronskowski, R.; Blochl, P. E. *J. Phys. Chem.* **1993**, *97*, 8617−8624.
(20) Andersen, O. K.; Jepsen, O. *Phys. Rev. Lett.* **1984**, *53*, 2571−2574.
(21) Jepsen, O.; Snob, M. *Linearized Band Structure Methods in Electronic Band-Structure and its Applications*; Springer Lecture Note; Springer-Verlag: Berlin, Germany, 1987.
(22) Tank, R.; Jepsen, O. *TB-LMTO-ASA Program*; Version 4.7; Max-Planck-Institut fur Festkorperforschung: Stuttgart, 2000.
(23) Blaha, P.; Schwarz, K.; Madsen, G.; Kvasnicka, D.; Luitz, J. *WIEN2k, An Augmented Plane Wave+ Local Orbitals Program for calculating Crystal Properties*; Technische Universität Wien: Vienna, Austria, 2001.
(24) Singh, D. J.; Nordstrom, L. *Planewaves, Pseudopotentials, and the LAPW Method*, 2nd ed.; Springer: New York, 2006.
(25) Madsen, G. K. H.; Blaha, P.; Schwarz, K.; Sjostedt, E.; Nordstrom, L. *Phys. Rev. B* **2001**, *64*, 195134/1−195134/9.
(26) Sjostedt, E.; Nordstrom, L.; Singh, D. J. *Solid State Commun.* **2000**, *114*, 15−20.
(27) Perdew, J. P.; Burke, K.; Ernzerhof, M. *Phys. Rev. Lett.* **1996**, *77*, 3865−3868.
(28) Marazza, R.; Rossi, D.; Ferro, R. *J. Less-Common Met.* **1988**, *138*, 189−193.
(29) Suzuki, H.; Yamaguchi, T.; Katoh, K.; Kasaya, M. *Phys. B* **1993**, *186−88*, 390−392.
(30) Schmidbaur, H.; Schier, A. *Chem. Soc. Rev.* **2008**, *37*, 1931−1951.
(31) Karpov, A.; Nuss, J.; Wedig, U.; Jansen, M. *J. Am. Chem. Soc.* **2004**, *126*, 14123−14128.
(32) Gibson, B. J.; Kremer, R. K.; Jepsen, O.; Garrett, J. D.; Hoffmann, R. D.; Pöttgen, R. *J. Phys.: Condens. Matter* **2001**, *13*, 3123−3137.
(33) Fornasini, M. L.; Iandelli, A.; Pani, M. *J. Alloys Compd.* **1992**, *187*, 243−247.

DOI: 10.1021/ja511394q
J. Am. Chem. Soc. 2015, 137, 1282−1289

(34) Pöttgen, R.; Hoffmann, R. D.; Mullmann, R.; Mosel, B. D.; Kotzyba, G. *Chem.—Eur. J.* **1997**, *3*, 1852−1859.
(35) Hoffmann, R. D.; Pöttgen, R.; Kussmann, D.; Mullmann, R.; Mosel, B. D. *Chem. Mater.* **2001**, *13*, 4019−4025.
(36) Manfrinetti, P.; Pani, A. *J. Alloys Compd.* **2005**, *393*, 180−184.
(37) Pani, M.; Manfrinetti, P.; Palenzona, A. *Intermetallics* **2009**, *17*, 146−149.
(38) Hermes, W.; Rodewald, U. C.; Chevalier, B.; Matar, S. F.; Eyert, V.; Pöttgen, R. *Solid State Sci.* **2010**, *12*, 929−937.
(39) Gibson, Q. D.; Schoop, L. M.; Muchler, L.; Xie, L. S.; Hirschberger, M.; Ong, N. P.; Car, R.; Cava, R. J. 2014, arXiv:1411.0005 [cond-mat.mtrl-sci], arXiv.org e-Print archive. http://arxiv.org/abs/1411.0005.
(40) Liang, T.; Gibson, Q.; Ali, M. N.; Liu, M.; Cava, R. J.; Ong, N. P. *Nat. Mater.* **2014**, DOI: 10.1038/NMAT4143.
(41) Deboer, F. R.; Bruck, E.; Nakotte, H.; Andreev, A. V.; Sechovsky, V.; Havela, L.; Nozar, P.; Denissen, C. J. M.; Buschow, K. H. J.; Vaziri, B.; Meissner, M.; Maletta, H.; Rogl, P. *Phys. B* **1992**, *176*, 275−287.
(42) Dwight, A. E. *Proc. Rare Earth Res. Conf., 12th* **1976**, *1*, 480.
(43) Flandorfer, H.; Hiebl, K.; Godart, C.; Rogl, P.; Saccone, A.; Ferro, R. *J. Alloys Compd.* **1997**, *256*, 170−174.
(44) Latka, K.; Gurgul, J. *Nucleonika* **2007**, *52*, S63−S66.
(45) Merlo, F.; Pani, M.; Fornasini, M. L. *J. Less-Common Met.* **1990**, *166*, 319−327.
(46) Mishra, T.; Schellenberg, I.; Eul, M.; Pöttgen, R. *Z. Kristallogr.* **2011**, *226*, 590−601.
(47) Sebastian, C. P.; Eckert, H.; Rayaprol, S.; Hoffmann, R. D.; Pöttgen, R. *Solid State Sci.* **2006**, *8*, 560−566.
(48) Sebastian, C. P.; Pöttgen, R. *Z. Naturforsch., B: J. Chem. Sci.* **2006**, *61*, 1045−1047.
(49) Tomuschat, C.; Schuster, H. U. *Z. Naturforsch., B: J. Chem. Sci.* **1981**, *36*, 1193−1194.
(50) Xie, L. S.; Schoop, L. M.; Medvedev, S. A.; Felser, C.; Cava, R. J. *Solid State Sci.* **2014**, *30*, 6−10.
(51) Pöttgen, R. *J. Mater. Chem.* **1995**, *5*, 505−508.

■ NOTE ADDED AFTER ASAP PUBLICATION

Figure 8 was corrected on January 16, 2015.

DOI: 10.1021/ja511394q
J. Am. Chem. Soc. 2015, 137, 1282−1289